Unusual Tuning of Mechanical Properties of Isotactic Polypropylene Using Counteraction of Shear Flow and β-Nucleating Agent on β-Form Nucleation

Yan-Hui Chen,[†] Gan-Ji Zhong,[†] Yan Wang,[†] Zhong-Ming Li,*,[†] and Liangbin Li[‡]

[†]*College of Polymer Science and Engineering and State Key Laboratory of Polymer Materials Engineering, Sichuan University, Chengdu 610065, China, and* [‡]*National Synchrotron Radiation Laboratory and Department of Polymer Science and Engineering, University of Science and Technology of China, Hefei 230026, China*

Introduction

Isotactic polypropylene (iPP) has good comprehensive properties, viz. easy processing, high heat resistance, and good stiffness, etc., and in turn is widely used as a commodity plastic. However, under conventional processing conditions, iPP crystallizes into sizable spherulites with few tie molecules between spherulites. With such a crystalline texture, iPP exhibits very low impact toughness, especially at lower temperature, which restricts its more extensive application. Therefore, toughening of iPP has always been an open research.[1] Up to now, four routes have been taken to improve impact strength of iPP, including copolymerizing with other olefin monomers,[2] blending with rubber or thermoplastic elastomer,[3] compounding with organic or inorganic fillers (e.g., nanoparticles),[4,5] and adding β-nucleating agent.[6−8] Without doubt, the modified iPP, more or less, increases its toughness.[2−8] The enhancement of toughness is, unfortunately, at sacrifice of other properties, e.g., strength, heat resistance, etc.[9] There are extremely few successful examples for simultaneously efficiently reinforcing and toughening iPP.[10,11]

It has been well established that for iPP oriented crystals (i.e., shish-kebabs) can bring out notable reinforcement on iPP,[10,11] while β-form crystals of iPP can greatly increase its toughness.[6−8,12] Flow (shear, elongational, or mixed) would induce formation of shish-kebabs whose content is governed to shear rate, shear duration, and molecular species and weight, etc.[13−17] On the other hand, β-form crystals can be high production generated by addition of β-nucleating agent under quiescent conditions.[7,18] This type of iPP crystals causes high toughness due to the β−α polymorphous transition and the loose structure of β-form crystals compared with α-crystals in favor of absorbing impact energy.[19,20] Naturally, an idea arises that combination of flow-induced molecular orientation crystallization and β-nucleant-induced β-form crystals produces efficient reinforcement and toughening on iPP. However, as a matter of fact, there is not any example of it in the open literature. The major reason is that the coexistence of a β-nucleating agent and a shear flow at above a certain but low level of shear rate depresses β-form nucleation.[21,22] Huo et al. performed a delicate study on iPP crystallization with β-nucleating agent and observed that as the shear rate rises, the content of β crystals constantly reduces, more

*To whom correspondence should be addressed. E-mail: zmli@scu.edu.cn.

greatly for higher nucleating agent content, showing counteraction between shear and β-nucleating agent for β-form formation.[22]

Apparently, it is a great practical challenge to prepare iPP parts with high molecular orientation and high β-crystal proportion for the purpose of both strength and toughness enhancement. In the present work, we attempt to fabricate iPP with considerably increased strength and toughness, for the first time, utilizing the counteraction of shear-induced orientation crystallization and β-nucleating agent on β-form nucleation. The crystallization process of iPP is manipulated by two stages: one is flow-induced crystallization for high molecular orientation, and the other is β-nucleating-agent-induced nucleation for high β-crystal content. More specifically, the oscillation shear supplied by an oscillation shear injection molding (OSIM) (its detailed definition is included in the Experimental Section) is imposed on β-nucleated iPP melt in the mold during injection molding. Initially, due to occurrence of shear flow and β-nucleating agent, β-form formation is restrained; thereby, the oriented α-crystals first form in the skin and intermediate layers of the sample. When the gate of the mold freezes, the shear ceases, and hereby, β-nucleating agent revives. The remainder of iPP melt in the core layer undergoes β-nucleation-induced crystallization. The results demonstrate that a large amount of shish-kebab structure appears in the surface and intermediate layers of the sample; at the same time, numerous β-form crystals form in the core layer, thus leading to prominent reinforcement and toughening for iPP.

Experimental Section

Materials. iPP, model T30S, was purchased from Dushanzi Petroleum Chemical Co., China, with a melt flow rate (MFR) of 3 g/10 min (230 °C, 21.6 N), $M_w = 39.9 \times 10^4$ g mol^{-1}, and $M_w/M_n = 4.6$. The β-nucleating agent is aryl amide compounds (TMB-5) and was supplied by Fine Chemical Institute, Shanxi, China.

Preparation of Nucleated iPP Samples. TMB-5 was first melt mixed with iPP in a twin-screw extruder to form a 1.0 wt % β-nucleating agent masterbatch. The masterbatch was further melt compounded with fresh iPP to produce iPP (pellets) with 0.2 wt % of TMB-5. The screw speed was fixed at 82 rpm, and the processing temperature profile was 170−180 °C from hopper to die. The iPP pellets were injection-molded into dumbbell bars in an injection temperature profile of 170−200 °C from hopper to nozzle. At packing stage of an injection molding cycle, the oscillation shear provided by the OSIM machine whose picture is available in the Supporting Information is continuously imposed on the melt. The primary feature of OSIM is that the hot melt is subjected to high pulse shear stress in the mold, which is given by two pistons moved reversibly at the same frequency. Generally, the OSIM can provide a peak shear rate in a single cycle from several s^{-1} up to hundreds of s^{-1}. In this work, the shear rate is about 220 s^{-1}. Only when the gate of the mold solidifies, the shear ceases. The conventional injection molding (CIM) was also carried out under the same processing conditions (only without oscillation shear) for comparison.

It is believed that the OSIM and CIM samples have a hierarchic structure, which gradually changes from outer to inner layer.[23,24] Accordingly, the sample was characterized layer by layer in the width direction. For the sake of brevity, the skin, intermediate, and core layers are referred to the layers from surface to ca. 0.5 mm deep, from 0.5 to ca. 1.5 mm, and from 1.5 to ca. 3.0 mm in the width direction (the total width is 6.0 mm), respectively.

Two-Dimensional Wide-Angle X-ray Diffraction (2D-WAXD) Measurement. To characterize the crystalline structure in the width direction using the two-dimensional wide-angle X-ray diffraction (2D-WAXD), we started with a 6.0 mm wide and 4.0 mm thick dumbbell tensile bar and machined away all of the tensile bar except for a 1.0 mm thick piece (the 6.0 mm width remains unchanged), as shown in Figure 1. The position of the sample obtained is located in the middle of the bar. The direction normal to MD−TD (the molding direction−transverse direction) plane was defined as ND. The X-ray beam with 1.0 mm width was perpendicular to the MD−TD plane, moved from exterior to inner, took a picture interval of 0.5 mm, and ceased in the position of 3.0 mm far from the edge because the remaining part was symmetrical, setting the first signal picture as surface layer which located in the range of 0−0.5 mm. The measurements were carried on the synchrotron light source (wavelength $\lambda = 0.14809$ nm) with the MarCCD as the detector at National Synchrotron Radiation Laboratory, China, and done in transmission geometry; meanwhile, the incident X-ray beam was set perpendicular to the flow direction. The scattered intensities were registered in the range of scattering angles 2θ from $11°$ to $22.5°$.

1D-WAXD profiles were obtained from circularly integrated intensities of 2D-WAXD image patterns acquired. Subsequently, through deconvoluting the peaks of 1D-WAXD profiles, the overall crystallinity X_c was calculated by

$$X_c = \frac{\sum A_{\text{cryst}}}{\sum A_{\text{cryst}} + \sum A_{\text{amorp}}} \qquad (1)$$

where A_{cryst} and A_{amorp} are the fitted areas of crystal and amorphous, respectively. The relative amount of the β-form crystal K_β was evaluated by the method of Turner-Jones et al.[25]

$$K_\beta = \frac{A_\beta(300)}{A_\beta(300) + A_\alpha(110) + A_\alpha(040) + A_\alpha(130)} \qquad (2)$$

$A_\beta(300)$ is the area of the (300) reflection peak; $A_\alpha(110)$, $A_\alpha(040)$, and $A_\alpha(130)$ are the areas of the (110), (040), and (130) reflection peaks, respectively. Meanwhile, the crystallinity of the β-form crystal X_β was given by

$$X_\beta = K_\beta X_c \qquad (3)$$

More details about WAXD data analysis are available in refs 13 and 22.

For evaluation of molecular orientation, the orientation parameter was calculated mathematically using Picken's method from the (040) reflection of WAXD for iPP.[26]

Scanning Electronic Microscopy (SEM). Permanganic etching was used for the samples surface for observation as described by Bassett et al.[27] The surfaces of all the samples were sputter-coated with a layer of gold to provide enhanced conductivity. Then the morphology was observed in an SEM, model JSM-5900LV, operating at 20 kV.

Differential Scanning Calorimetry (DSC). It was performed using a Star system with a constant heating rate of 10 °C min^{-1} under a nitrogen atmosphere. The data were collected from 40 to 200 °C, and the sample weight was about 5−10 mg.

Mechanical Property Tests. The tensile test was performed at 23 °C according to ASTM D-638 at a cross-head speed of 50 mm min^{-1}, while to evaluate the tensile modulus, a draw speed of 5 mm min^{-1} was applied. The notched impact test was carried out at 23 ± 2 °C according to the standard GB/T 1843-96. The testing samples had the dimension $60 \times 6 \times 4$ mm^3 with a V-notch of 1.2 mm depth.
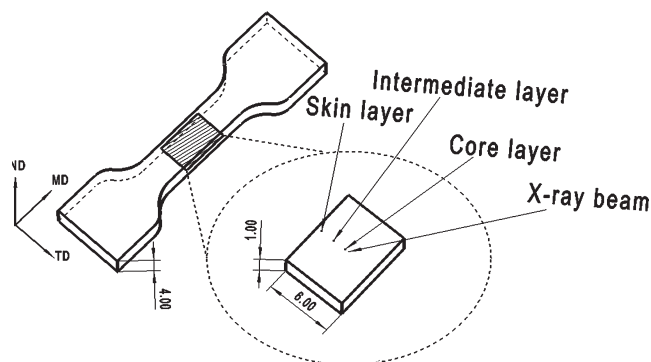

Figure 1. Schematic diagram of the positions of the samples for WAXD measurement: MD, the molding direction (i.e., flow direction); TD, the transverse direction; ND, the direction normal to the MD−TD plane.
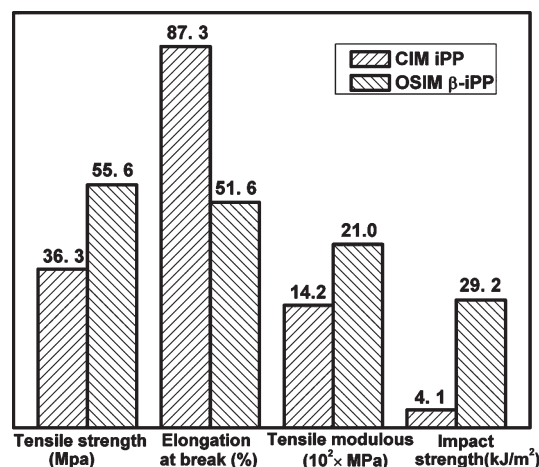

Figure 2. Comparison of the mechanical properties including tensile strength, elongation at break, tensile modulus, and impact strength for CIM iPP and OSIM β-iPP bars with 0.2 wt % β-nucleating agent.

Results

Mechanical Properties. Compared with CIM iPP samples, OSIM β-iPP samples exhibit superior mechanical properties as shown in Figure 2. The tensile strength of OSIM β-iPP samples reaches 55.6 MPa, which is 19.3 MPa higher than that of CIM iPP samples (36.3 MPa). The impact strength of OSIM β-iPP samples (29.2 kJ/m^2) is over 7 times that of CIM iPP samples (4.1 kJ/m^2), showing super tough and brittle transition between these two samples. The tensile modulus rises from 1.42 to 2.10 GPa. Only the elongation at break decreases from 87.3% to 51.6%, but it still fractures in a ductile manner. These data indicate that the mechanical properties of OSIM β-iPP fall into the range of engineering plastics. Hence, conclusions can be safely obtained that, by means of the counteraction of shear-induced molecular orientation crystallization and β-nucleating-agent-induced β-form crystals, the simultaneous reinforcement and toughening of iPP have been successfully achieved.

It is worth pointing out that the samples of pure iPP using OSIM (OSIM iPP) and iPP with 0.2 wt % β-nucleating agent using CIM (CIM β-iPP) are also prepared in our reference experiments. However, the former has improved tensile strength while the increment of the impact strength is less than that of OSIM β-iPP; in contrast, the latter has improved impact strength while tensile strength decreases. Both of them cannot achieve the best properties and are not discussed here. Hereinafter, the CIM iPP and OSIM β-iPP samples are chosen for comparison to investigate their structures and morphology
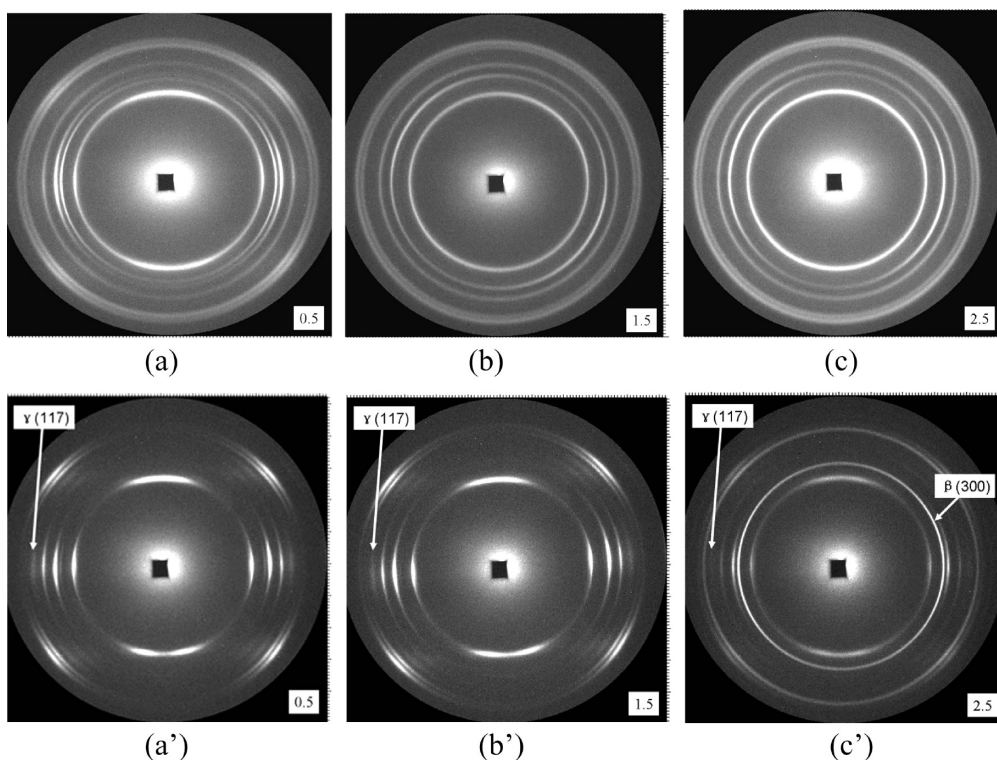
Figure 3. 2D-WAXD patterns of skin layer (a, a′), intermediate layer (b, b′), and core layer (c, c′) of CIM iPP (a, b, c) and OSIM β-iPP (a′, b′, c′). The number of each picture represents the distance to the edge of samples (mm).

by DSC, 2D-WAXD, and SEM and, furthermore, to understand their structure−property relationship.

Crystalline Structure. Figure 3 shows the selected 2D-WAXS patterns from different layers, viz. skin, intermediate, and core layers. For intermediate and core layers of CIM iPP (Figure 3b,c), the diffraction intensity distribution consists of five diffraction rings associated with different lattice planes of iPP, including (110), (040), (130), (111), and ($\bar{1}$31), from inner to outer circles, respectively, which are characteristic of α-phase crystals. For skin layer (Figure 3a), additional (300) and (311) lattice planes appear, corresponding to the reflection of β-phase. Furthermore, the arclike diffractions are clearly seen in the skin layer's pattern indicative of molecular orientation of iPP but are absent in the intermediate and core layers.

Shear-induced β-phase formation and molecular orientation have been thoroughly investigated.[13,19,28] Generally, shearing of iPP melt causes formation of α-row nuclei and then a subsequent growth of the β-phase on the formed α-row nuclei,[13] which can explain the presence of β-form crystals and molecular orientation in the skin layer as compared to the intermediate and core layers of CIM iPP; although the shear stress is also existent for the melt in the intermediate and core layers, the slow solidifying rate leaves enough time for the relaxation of extended iPP chains, and finally iPP crystallizes in α-phase from an isotropic melt. It can be seen more vividly that β-crystals and molecular orientation exist in the skin layer, as shown in Figure 4a as well as Tables 1, and 2, but due to short shearing duration and relaxation, both have a low level, e.g., 0.082 for β-crystal fraction and 0.683 for orientation degree in 0.5 mm deep layer. We also noticed that in the core layer there is a very tiny (300) reflection for β-form, corresponding to β-form fraction of 0.009, but it is almost a negligible level so it is not considered.

Compared with CIM iPP samples, there is an obvious azimuthal diffraction intensity in every layer of OSIM
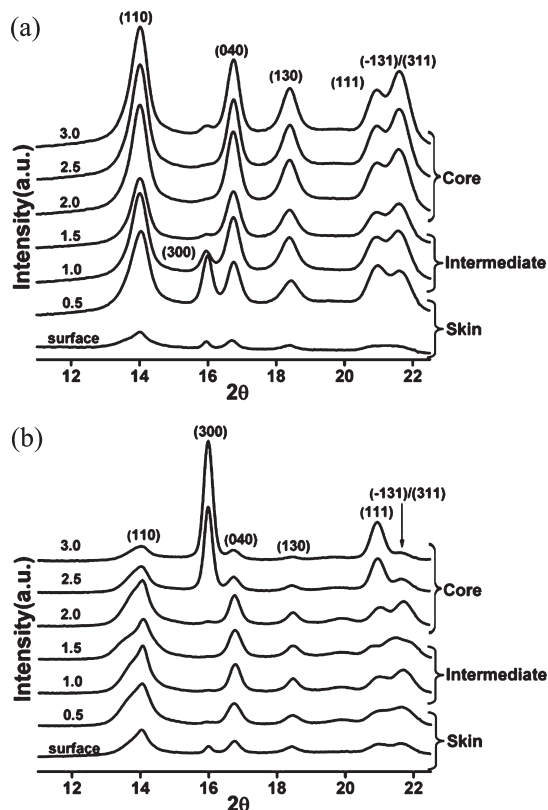

Figure 4. 1D-WAXD curves obtained from circularly integrated intensities of 2D-WAXD patterns in Figure 3: (a) CIM iPP, (b) OSIM β-iPP.

β-iPP sample (Figure 3a′−c′), which indicates the strong orientation of molecular chains throughout the sample. The orientation should undoubtedly be ascribed to the oscillation shear on the melt before the gate of the mold freezes.

**Table 1. β-Form Crystal Fraction Obtained from Its 1D-WAXD (Figure 3)**

position	depth from surface (mm)	CIM iPP	OSIM β-iPP
skin	surface	0.181	0.132
	0.5	0.082	0
intermediate	1.0	0.033	0
	1.5	0	0
core	2.0	0	0
	2.5	0	0.290
	3.0	0.009	0.435

Table 2. Degree of Orientation Fitted from the Intensity of α (040) along Azimuthal Angle

position	depth from surface (mm)	CIM iPP	OSIM β-iPP
skin	surface	0.732	0.946
	0.5	0.683	0.973
intermediate	1.0	0	0.976
	1.5	0	0.969
core	2.0	0	0.962
	2.5	0	0.947
	3.0	0	0.924
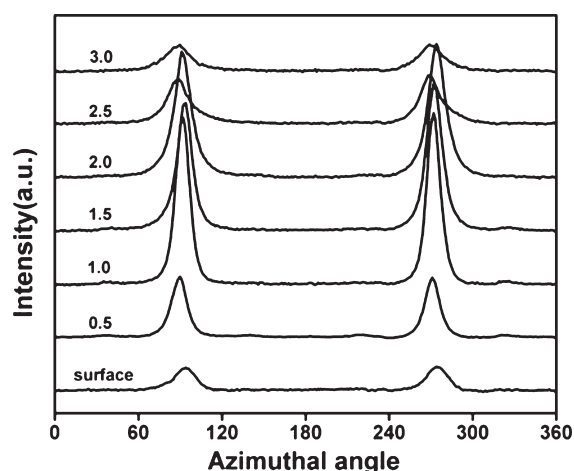
Figure 5. Intensity distribution of α (040) along azimuthal angle calculated mathematically using Picken's method from the (040) reflection of 2D-WAXD for OSIM β-iPP.

As expected, strong reflections of β-crystals emerge in the core layer (indicated by an arrow in Figure 3c′). This phenomenon definitely verifies that combination of shear field and β-nucleating agent suppresses the formation of β-crystals in the skin and intermediate layers. In the core layer, as the gate of the mold freezes, iPP is still in the melt state, so that the molecular chains have sufficient time to relax. In this case, the β-nucleating agent takes effect, leading to β-phase. Clearer characterization is shown in Figure 4b. The fraction of β-crystals is up to 0.290 and 0.435 and occupies 49% and 74% of the total crystallinity (0.590) for 2.5 mm and 3.0 mm deep layers (core layer), respectively, as seen in Table 1. Apparently, the high β-crystal content greatly contributes to the toughness of OSIM samples. Furthermore, a low level of β-crystal also appear in the surface, which is lower than the surface layer of CIM sample and is, apparently, the result from compromise of shearing effect and β-nucleant.[22] The degree of orientation for OSIM samples responsible for strength is rather high in every layer, and the highest appears in the intermediate layer (Figure 5 and Table 2). It is interesting to note fading tiny arcs of the γ-phase crystals at the equator of the diffraction patterns for the OSIM samples as well (shown by an arrow in Figure 3a′−c′). This little amount of γ-phase is also visible in
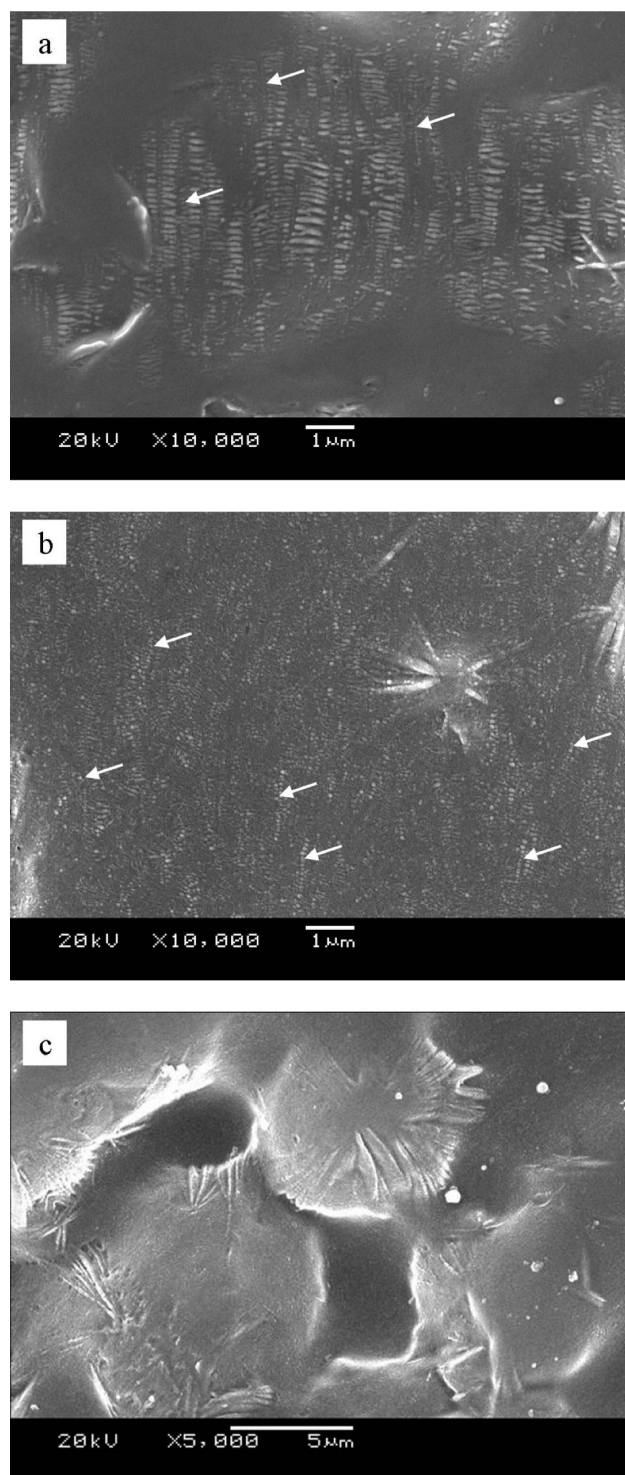
Figure 6. SEM photographs of OSIM β-iPP sample: (a) skin layer, (b) intermediate layer, and (c) core layer.

the integrations in Figure 4b as the broad (117) peak between the (130) and (111) peaks. It was reported that the occurrence of γ-phase was mainly associated with high molecular orientation and high pressure.[29] In our case, γ-form crystals appear in the OSIM sample, which can be ascribed to a combination of the local high pressure and shear.

Crystalline Phase Morphology. Figure 6 shows the crystalline phase morphology of OSIM sample. It displays oriented crystals, i.e., shish-kebabs, in the skin and intermediate layers (as examples, some are indicated by arrows in Figure 6a,b). In the core layer, the typical spherulites are
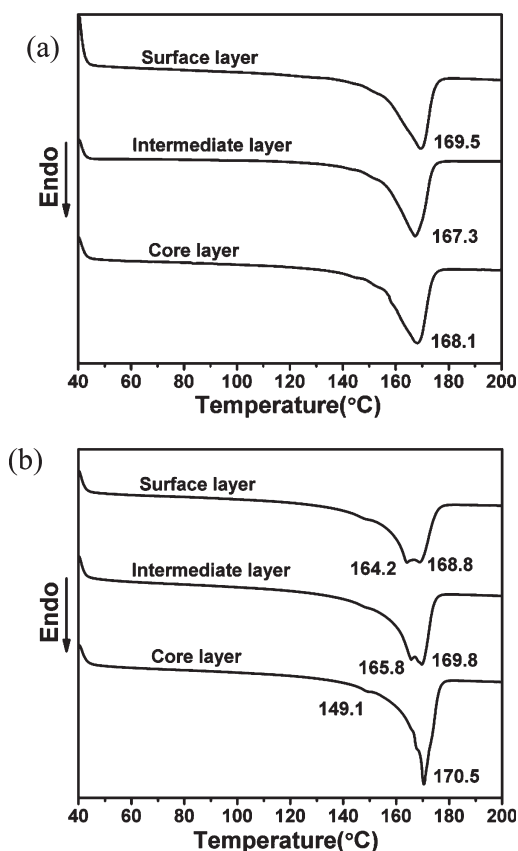
Figure 7. DSC heating curves of CIM iPP (a) and OSIM β-iPP samples (b).

observed. Though a high level of molecular orientation exists in the core layer of OSIM samples (Table 2), one can hardly see the shish-kebab structure in this layer.

Thermal Behavior. Figure 7 shows DSC heating curves of CIM and OSIM samples. For CIM sample, every layer shows one obvious endothermic peak of α-phase and a shallow peak of β-phase between 140 and 150 °C.[30] In contrast, the skin and intermediate layers of OSIM sample show two endothermic peaks of α-phase, which represent α-form lamellar crystals and stretched α-form crystals, respectively. It is worth mentioning that in the core layer of OSIM sample one obvious endothermic peak appears at the temperature of about 149.1 °C attributed to melting of β-phase of iPP,[19] which is induced by β-nucleating agent, while the other one is the endothermic peak of α-phase. This phenomenon once again verifies that the shear field suppresses the activity of β-nucleating agent but induces the formation of α-crystals in the skin and intermediate layers. From DSC and WAXD results, we deduce that the crystal form of shish-kebab structure in the skin and intermediate layers (Figure 6a,b) is α-crystal.

Discussion

The results reported above indicate the objective to simultaneously reinforce and toughen iPP has been successfully achieved by utilizing the counteraction of shear and β-nucleant on β-modification nucleation and demonstrates the generation of the predesigned morphology and structure in the samples.

Shear-induced crystallization has always been a hot spot for decades.[31−34] Shear may induce formation of oriented crystals, i.e., shish-kebabs,[16,33] which is the most fascinating feature, although its molecular mechanism needs to be clarified.[33,34] Our study is one of good examples for shear-induced crystallization applying to factual polymer processing.[35] In the process

of CIM, the melt is filled into the cool mold quickly and becomes sheared melt due to high flow rate during mold filling. When it encounters the cool mold surface, a thin layer is frozen owing to fast crystallization at high supercooling. So the molecular orientation is preserved, which is verified by the WAXD result for the skin layer of CIM sample (Table 2). As the mold cavity is fully filled, the melt goes through nonisothermal crystallization and forms α-form crystals for pure iPP (Figure 3b,c). The case in OSIM operation is quite different, in which the oscillation shear is applied at the packing stage. The shear-induced crystallization starts to gradually form thick oriented layer with the highest orientation degree (0.5−2.0 mm deep layers, Table 2). It should be noted that comparison of the orientation degree of skin layer for CIM and OSIM samples shows that the OSIM sample is higher, which implies that the molecular orientation of the specific positions (surface and 0.5 mm deep layer) for structure measurement includes the contribution of the oscillation shear. This can be understandable because the oscillation shear flow also has an effect on mixing the melt, so even though in the same thick position, the solidification of the OSIM samples falls behind the CIM sample. Generally, the interior layer has more time for oriented nuclei formation than the outer layer, so the amount of the shish-kebabs formed in the intermediate layer is larger than in the skin layer (Figure 6a,b). When the gate of the mold is frozen, the shear stops. From then on, the sheared melt continues to crystallize under quiescent conditions, and at the same time, the oriented molecules or network relax. The relaxation of molecules is intensified by the previous shear-induced viscous heat. The disoriented chains form pointlike nuclei and develop into spherulites. Nevertheless, we believe that a small amount of oriented nuclei formed during shear duration still survive in the core layer, which have a high orientation degree, but, quite possibly, induce isotropic growth in the unoriented melt. This can be demonstrated by Figure 5, in which the intensity distribution peak along the azimuthal angle is much weaker in the core layer than that in the intermediate layer of the OSIM sample. Now we come to the possible reasons for the concurrence of molecular orientation (Table 2) and typical spherulites (Figure 6c) in the core layer of OSIM sample. Despite crystallization under quiescent conditions, initially, there must exist some oriented nuclei formed at shearing stage, whose quantity and size depend on the supercooling (cooling rate) and the shear rate. The oriented nuclei partially remain, which are too small to observe with SEM but, indeed, give rise to the molecular orientation. On the other hand, the SEM image exhibits larger scale aggregate state structure of crystals while 2D-WAXD indicates the oriented structure, either molecular chains or segments. There may be mainly orientation of molecular chain segments in the core layer, which exists in the resultant crystals in some forms.

The β-crystals in iPP can be obtained by addition of certain heterogeneous nucleating agents,[6−8] by crystallization in a temperature gradient,[12] or by shear-induced crystallization.[13] The effective and accessible method to obtain the iPP with higher level of β-phase is addition of some β-nucleating agents. During shear-induced crystallization of pure iPP, the α-row nuclei formed in situ induces the growth of the β-form. On the basis of this, one can understand the presence of β-form iPP in the skin layer of the CIM sample (Figure 3a and Table 1). One attractive result in our work is that in the β-nucleated OSIM sample molded in the industrial equipment β-form crystals are absent in the high shear layer (intermediate) while they indeed appear in the core layer, though shear and β-nucleating agent separately facilitate β-form crystal formation. Varga[21] first found that the high shear rate restrained the formation of β-iPP. Huo et al.[22] studied the same phenomenon and argued that the shear accelerates the nucleation and the growth of α-row nuclei which was more active to induce the formation of α-crystals instead of β-crystals in

the presence of β-nucleating agent; as a consequence, this acceleration restrains the growth of the β-phase. The higher shear rate prevents the formation of β-iPP more strongly. In our case, there is no any trace of β-crystals in the intermediate layer of OSIM β-iPP samples, which means that the applied oscillation shear completely suppresses the β-nucleating agent, and in the meantime, α-row-nuclei-induced β-crystals do not yet occur. The molecular mechanism underlying this amazing phenomenon needs further work to clarify. Presumably, the very high shear strength and unique thermodynamic process for crystallizing molecular chains are responsible for it. On one hand, counteraction of oscillation shear and β-nucleating agent depresses formation of β-form crystals, but quite possibly, this cannot completely diminish them, which can be confirmed by the result of Huo et al.[22] and also the existence of β-form in the surface of the OSIM β-iPP sample. On the other hand, in the cool mold, only as the supercooling is enough or the dynamical condition is met, the nuclei formation and crystal growth take place, and subsequently the crystallizing chains stack onto the surface of the solidified layer. In other words, there is a liquid−solid interface where the highest shear rate exists. Under the influence of the intense shear near the solidified surface, the as-formed and immature crystals which tend to be static are elongated under the action of the drawing from neighboring and moving molecules. Upon stretching, the transition from the metastable β-phase to stable α-phase will happen.[7] Both effects account for the absence of β-phase in the intermediate layers (Figures 3b′ and 4b). In the surface, because the shear is not enough and no $\beta-\alpha$ form transition takes place, a small β-phase fraction is thus obtained (Table 2). As the oscillation shear stops, β-nucleating agent revives. Eventually, typical β-phase crystals are obtained in the core layer (Figures 3c′ and 4b).

In summary, we have successfully controlled the structure and morphology formation of iPP during a typical polymer processing and tuned its mechanical properties. The competition of shear-induced crystallization and β-nucleant results in the hierarchic structure of the OSIM β-iPP sample, which perfectly accounts for its superb mechanical properties. The outer layers (skin and intermediate layers) with highly oriented α-form crystals (shish-kebabs) endows the high strength and modulus, while the core layer with high-proportion β-form spherulites causes good toughness. This unique structure of the OSIM β-iPP sample reminds of the bamboo-like bionic structure with tight and fibrillar outer layer as well as soft and loose inner layer. From the point of view of mechanical properties, it is an excellent combination of strength and toughness. Our attempt opens up a door toward achieving high-performance polymer materials based on commodity plastics by a new manipulation strategy for structure and morphology. Additionally, a plastic engineer should keep in mind that addition of β-nucleating agent cannot always help improve toughness if the iPP material is continuously subjected to dramatic flow field during processing.

Supporting Information Available: Overall picture of oscillation shear injection molding machine as well as local and 3D schematic pictures for mold with oscillation shear supplier. This material is available free of charge via the Internet at http://pubs.acs.org.

References and Notes

(1) Grein, C. *Adv. Polym. Sci.* **2005**, *188*, 43.
(2) Galli, P.; Vecellio, G. *Prog. Polym. Sci.* **2001**, *26*, 1287.
(3) Bucknall, C. B.; Soares, V. L. P.; Yang, H. H.; Zhang, X. C. *Macromol. Symp.* **1996**, *101*, 265.
(4) Karnani, R.; Krishnan, M.; Narayan, R. *Polym. Eng. Sci.* **1997**, *37*, 476.
(5) Thio, Y. S.; Argon, A. S.; Cohen, R. E.; Weinberg, M. *Polymer* **2002**, *43*, 3661.
(6) Varga, J. *J. Macromol. Sci., Phys.* **2002**, *41*, 1121.
(7) Chen, H. B.; Karger-Kocsis, J.; Wu, J. S.; Varga, J. *Polymer* **2002**, *43*, 6505.
(8) Varga, J.; Menyhárd, A. *Macromolecules* **2007**, *40*, 2422.
(9) Wang, Y.; Zhang, Q.; Na, B.; Du, R. N.; Fu, Q.; Shen, K. Z. *Polymer* **2003**, *44*, 4261.
(10) Kalay, G.; Bevis, M. J. *J. Polym. Sci., Part B: Polym. Phys.* **1997**, *35*, 241.
(11) Schrauwen, B. A. G.; Breemen, L. C. A. V.; Spoelstra, A. B.; Govaert, L. E.; Peters, G. W. M.; Meijer, H. E. H. *Macromolecules* **2004**, *37*, 8618.
(12) Lovinger, A. J.; Chua, J. O.; Gryte, C. C. *J. Polym. Sci., Polym. Phys. Ed.* **1977**, *15*, 641.
(13) Somani, R. H.; Hsiao, B. S.; Nogales, A.; Fruitwala, H.; Srinivas, S.; Tsou, A. H. *Macromolecules* **2001**, *34*, 5902.
(14) Kumaraswamy, G.; Issaian, A. M.; Kornfield, J. A. *Macromolecules* **1999**, *32*, 7537.
(15) Li, L. B.; de Jeu, W. H. *Macromolecules* **2003**, *36*, 4862.
(16) Zhu, P. W.; Edward, G. *Macromolecules* **2004**, *37*, 2658.
(17) Gutierrez, M. C. G.; Alfonso, G. C.; Riekel, C.; Azzurri, F. *Macromolecules* **2004**, *37*, 478.
(18) Tjong, S. C.; Shen, J. S.; Li, R. K. Y. *Polymer* **1996**, *37*, 2309.
(19) Varga, J.; Karger-Kocsis, J. *J. Polym. Sci., Part B: Polym. Phys.* **1996**, *34*, 657.
(20) Ferro, D. R.; Meille, S. V.; Brckner, S. *Macromolecules* **1998**, *31*, 6926.
(21) Varga, J. *J. Therm. Anal.* **1989**, *35*, 1891.
(22) Huo, H.; Jiang, S. J.; An, L. J.; Feng, J. C. *Macromolecules* **2004**, *37*, 2478.
(23) Zhu, P. W.; Phillips, A.; Tung, J.; Edward, G. *J. Appl. Phys.* **2005**, *97*, 104908.
(24) Zhong, G. J.; Li, Z. M.; Li, L. B.; Mendes, E. *Polymer* **2007**, *48*, 1729.
(25) Turner-Jones, A.; Cobbold, A. *J. Polym. Lett.* **1968**, *6*, 539.
(26) Picken, S. J.; Aerts, J.; Visser, R.; Northolt, M. G. *Macromolecules* **1990**, *23*, 3849.
(27) Olley, R. H.; Bassett, D. C. *Polymer* **1982**, *23*, 1707.
(28) Kumaraswamy, G.; Korneld, J. A.; Yeh, F.; Hsiao, B. S. *Macromolecules* **2002**, *35*, 1762.
(29) Kalay, G.; Zhong, Z. P.; Allan, P.; Bevis, M. J. *Polymer* **1996**, *37*, 2077.
(30) Karger-Kocsis, J.; Varga, J. *J. Appl. Polym. Sci.* **1996**, *62*, 291.
(31) Korneld, J. A.; Kumaraswamy, G.; Issaian, A. M. *Ind. Eng. Chem. Res.* **2002**, *41*, 6383.
(32) Hsiao, B. S.; Yang, L.; Somani, R. H.; Avila-Orta, C. A.; Zhu, L. *Phys. Rev. Lett.* **2005**, *94*, 117802.
(33) Kimata, S.; Sakurai, T.; Nozue, Y.; Kasahara, T.; Yamaguchi, N.; Karino, T.; Shibayama, M.; Korneld, J. A. *Science* **2007**, *316*, 1014.
(34) Janeschitz-Kriegl, H.; Eder, G. *J. Macromol. Sci., Phys.* **2007**, *46*, 591.
(35) Housmans, J. W.; Gahleitner, M.; Peters, G. W. M.; Meijer, H. E. H. *Polymer* **2009**, *50*, 2304.